Scientific paper

Preparation, Characterization and Theoretical Calculation of a Cadmium Complex of 3-hydroxy-2-methylquinolin-4-carboxylate and 1,10-phenanthroline

Ting-Qun Qiu[1], Zhi-Tao Lu[1], Zi-Jian He[1], Zheng-Ping Xie[2], Jin Guo[1]* and Xiu-Guang Yi[1]*

[1] *School of Chemistry and Chemical Engineering, Jinggangshan University, Ji'an 343009, PR China*

[2] *School of Chemistry and Chemical Engineering, Jiangxi University of Science and Technology, Ganzhou 341000, PR China*

* *Corresponding author: E-mail: E-mail: 39366276@qq.com jayxgggchem@163.com*

Received: 09-30-2024

Abstract

A novel organic-inorganic hybrid cadmium complex [Cd(MCA)$_2$(Phen)(H$_2$O)] (MCA = anion of 3-hydroxyquinoline-4-carboxylic acid; Phen = 1,10-phenanthroline) was synthesized by solvothermal method and characterized by single crystal X-ray diffraction. The complex exhibits a two-dimensional structure through hydrogen bonding and π···π packing interactions. Solid state photoluminescence specter shows that the complex displays an emission in the red region of the light spectrum that time-dependent density functional theory calculations reveal can be attributed to ligand-to-ligand charge transfer. Solid diffuse reflection specter shows that the energy band gap of the complex is 2.32 eV.

Keywords: Cadmium, crystal structure, solid state diffuse reflection, TDDFT.

1. Introduction

Due to their unique physical and chemical properties and wide application prospects, metal-organic complexes have shown extraordinary potential and value in many fields such as material science,[1,2] catalytic chemistry,[3,4] biomedicine,[5,6] photoelectric technology and so on.[7,8] These complexes are usually formed by metal ions or atoms binding to organic ligands through coordination bonds. Their structural diversity, adjustability, and functionality make them star molecules in scientific research and technological applications.

Quinolinecarboxylic acid,[9–11] as a nitrogen-containing heterocyclic aromatic carboxylic acid compound, its unique structure gives it superior properties as a metal-organic complex ligand. The carboxyl group in quinolinecarboxylic acid can be coordinated with metal ions in many ways, such as monodentate, bidentate or bridged. The nitrogen atom on the quinoline ring also has certain coordination ability and can form additional coordination bonds with metal ions, further enriching the structural types and properties of the complexes. The rigid planar structure of the quinoline ring and the high reactivity of carboxyl group enable quinoline carboxylic acid to form stable and structurally diverse complexes with various metal ions.

Transition metals can be combined with many ligands to form complex and functional complexes due to their unfilled *d* orbitals, variable oxidation states and high coordination number.[12–14] These complexes play an important role in catalysis, medicine, materials science and other fields, and promote the rapid development of related fields.[15,16]

Based on this, we are interested in crystal engineering of compounds containing group 12 elements with 3-hydroxy-2-methylquinolin-4-carboxylic acid (HMCA) as ligand.[17] We report the solvothermal synthesis, X-ray crystal structure, photoluminescence and UV-visible diffuse reflectance spectral properties of a novel cadmium complex with a neutral isolated (0D) structure, and time-dependent density functional theory (TDDFT) calculations [Cd(MCA)$_2$(Phen)(H$_2$O)].

2. Experiment

2. 1. Materials and Instruments

All reagents and chemicals are reagent grade, commercially available, and used directly for the reaction. The infrared spectrum of KBr disk was analyzed by PE-1 FT-IR spectrometer. Solid state UV/VIS diffuse reflection spectroscopy was performed on a computer-controlled TU1901 UV/VIS spectrometer. The fine ground powder was coated with barium sulfate to obtain 100% reflectance. The photoluminescence characteristics were studied on the F97XP photoluminescence spectrometer.

2. 2. Synthesis of 3-hydroxy-2-methylquinoline-4-carboxylic acid (HMCA)

Synthesis of isatin: Indigo (0.262 g, 1.0 mmol), $K_2Cr_2O_7$ (0.147 g, 0.5 mmol) and distilled water (200 mL) were added to 500 mL three-neck flask and stirred. After cooling, dilute H_2SO_4 (10%, 250 mL) was added, stirred at 43°C for 1.5 h, diluted with twice the volume of distilled water, filtered out, dissolved in 10% NaOH solution, filtered again, and neutralized with 10% HCl until pH = 7.[18] Yield: 0.23 g (90%); m.p. 210°C; HRMS *m*/*z* (ESI): calculated for $C_8H_5NO_2$ $[M+H]^+$ 147.0320, found 147.0826.

Synthesis HMCA: Isatin (0.147 g, 1.0 mmol) obtained in the previous step was added to the distilled water solution (200 mL) of NaOH (0.02 g, 0.5 mmol) to and filter. The filtrate and NaOH (0.02 g, 0.5 mmol) were added to chloracetone (0.092 g, 1.0 mmol), and hydrochloric acid was added to adjust pH = 7, and filtration was done. Yield: 0.096 g (95%); m.p. 225°C; HRMS *m*/*z* (ESI): calculated for $C_{11}H_9NO_3$ $[M+H]^+$ 203.0582, found 203.0548. ^{1}H NMR (400 MHz, DMSO) δ 9.15 (s, 1H), 7.93 (d, *J* = 8.0 Hz, 1H), 7.64 (t, *J* = 8.0 Hz, 1H), 7.60 7.52 (m, 2H), 2.70 (s, 3H).

2. 3. Synthesis of Title Complexes

The ligand HMCA (0.1015 g, 0.5 mmol), cadmium acetate dihydrate (0.267 g, 1.0 mmol) and Phen (0.1 g, 0.5 mmol) were accurately weighed, and the above weighed samples were put into a 20 mL glass vial, followed by 10 mL water and 5 mL ethanol, and stirred with a glass rod. The substance in the glass bottle is placed in the oven at 80°C for four days. After cooling the mixture slowly down to room temperature, reddish block crystals suitable for X-ray analysis were collected and washed. Yield: 70% (based on cadmium). IR (KBr, cm^{-1}): 3420 (vs), 3044 (w), 2921 (w), 1592 (vs), 1516 (vs), 1423 (vs), 1355 (m), 1313 (m), 1216 (m), 1148 (m), 1094 (m), 1009 (m), 849 (vs), 777 (vs), 722 (vs), 642 (vs); Anal. Calcd. for $C_{34}H_{26}CdN_4O_7$ (%): C 57.11; H 3.67; N 7.84. Found (%): C 57.12; H 3.61; N 7.85.

2. 4. X-ray Structure Determination

The single-crystal X-ray diffraction data set of the complex **1** was obtained by using a SuperNova CCD X-ray diffractometer. The micro-focus sealed X-ray tube is radiation source has Mo-*Kα* radiation with being λ of 0.71073 Å. A mirror is acted as the diffraction radiation monochromator. The absorption corrections for complex **1** was made using the CrysAlis PRO programs.[19] The structure of complex **1** was solved *via* direct method and subsequently refined using SHELXT and SHELXL programs, respectively[20,21] with the OLEX2 graphical interface.[22] All non-hydrogen atoms were located on the respective difference Fourier maps and anisotropically refined, while hydrogen atoms were theoretically found, allowed to attach on the parent atoms and isotropically refined. Selected crystal data and structural refinement details of the complex **1** are listed in Table 1. The selected bond lengths (Å) and bond angles (°) are listed in Table 2 and hydrogen bond interactions are shown in Table 3.

Table 1. Crystallographic data and structural analysis of the complex 1

Empirical formula	$C_{34}H_{26}CdN_4O_7$
Formula weight	714.99
Temperature/K	293
Crystal system	triclinic
Space group	*P*–1
a/Å	9.6365(3)
b/Å	12.8942(4)
c/Å	13.6041(5)
α/°	108.980(3)
β/°	98.922(3)
γ/°	102.637(3)
Volume/Å^3	1512.14(9)
Z	2
ρ_{calc}g/cm^3	1.570
μ/mm^{-1}	0.779
F(000)	724.0
Reflections collected	13170
Independent reflections (R_{int})	6956 (0.0225)
Data/restraints/parameters	6956/0/420
Goodness-of-fit on F^2	1.044
R_1, wR_2 $[I > 2\sigma(I)]$	0.0391, 0.0772
R_1, wR_2 (all data)	0.0530, 0.0843
Largest diff. peak/hole / e Å^{-3}	0.53/–0.34

3. Results and Discussion

3. 1. Crystal Structure Analysis of Complex

X-ray single-crystal diffraction analysis reveals that the complex **1** that crystallizes in the triclinic system space group *P*–1 and is composed of a neutral isolated molecule as shown in Figure 1. The cadmium ion is surrounded by four oxygen atoms from two HMCA molecules, two nitrogen at-

oms from the auxiliary ligand, and one oxygen atom from water molecule, forming a seven-coordination structure mode. The observed Cd–O bonds lengths in the range 2.2774(19)–2.458(2) Å and Cd–N bond lengths in the range 2.342(2)–2.357(2) Å are comparable with those reported in the references.[23,24] In the complex **1**, there are several O–H···O, O–H···N, C–H···O hydrogen-bonding interactions that allow the construction of a 3D supramolecular framework (the intramolecular hydrogen bond for O1–H1···O2, O4–H4···O5, C10–H10···O3, C21–H21···O6 and the intermolecular hydrogen bond for O7–H7A···N2^{i}, O7–H7B···O2^{ii}; C8–H8···O1^{iii}), as shown in Table 3 and Figure 2.

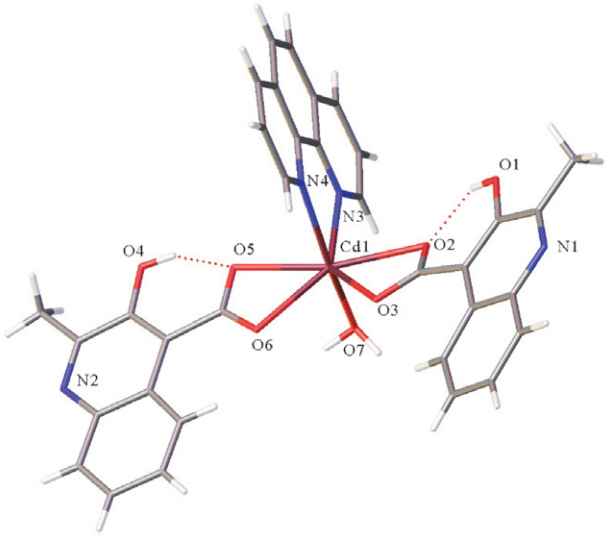

Figure 1. Intramolecular hydrogen bonds present in the complex 1

Table 2. Selected bond lengths (Å) and bond angles (°) for the complex 1

Distance	Length/Å	Distance	Length/Å
Cd1–O2	2.445(2)	Cd1–O7	2.2774(19)
Cd1–O3	2.3519(19)	Cd1–N3	2.357(2)
Cd1–O5	2.458(2)	Cd1–N4	2.342(2)
Cd1–O6	2.366(2)		
Angle	**(°)**	**Angle**	**(°)**
O2–Cd1–O5	166.62(7)	O2–Cd1–C1	27.59(7)
O3–Cd1–O2	54.15(7)	O3–Cd1–O5	137.41(7)
O3–Cd1–O6	86.12(7)	O3–Cd1–N3	137.51(7)
O3–Cd1–C1	26.69(8)	O5–Cd1–C1	162.43(8)
O6–Cd1–O2	139.51(7)	O6–Cd1–C1	112.74(8)
O7–Cd1–O2	94.08(7)	O7–Cd1–O3	104.99(8)
O7–Cd1–O5	88.76(7)	O7–Cd1–O6	88.63(8)
O7–Cd1–N3	88.63(8)	O7–Cd1–N4	159.53(9)
O7–Cd1–C1	102.70(8)	N3–Cd1–O2	85.40(7)
N3–Cd1–O5	81.60(7)	N3–Cd1–O6	135.09(7)
N3–Cd1–C1	111.57(8)	N4–Cd1–O2	88.83(8)
N4–Cd1–O3	93.14(8)	N4–Cd1–O5	84.06(7)
N4–Cd1–O6	102.23(8)	N4–Cd1–N3	71.39(8)
N4–Cd1–C1	89.18(8)		

Table 3. Hydrogen bond lengths (Å) and bond angles (°) in 1

D–H···A (°)	D–H (Å)	H···A (Å)	D···A (Å)	D–H···A
O1–H1···O2	0.82	1.86	2.577(3)	145
O4–H4···O5	0.82	1.75	2.474(3)	146
O7–H7A···N2^{i}	0.86	1.92	2.756(3)	162
O7–H7B···O2^{ii}	0.86	2.31	2.782(3)	115
C8–H8···O1^{iii}	0.95(3)	2.59(3)	3.387(4)	142(3)
C10–H10···O3	0.92(3)	2.33(3)	2.911(4)	121(2)
C21–H21···O6	0.92(3)	2.33(3)	2.880(3)	127(2)

Symmetry codes: (i) 1 – *x*, 2 – *y*, 2 – *z*; (ii) 1 + *x*, *y*, *z*; (iii) 1 – *x*, 2 – *y*, 1 – *z*.

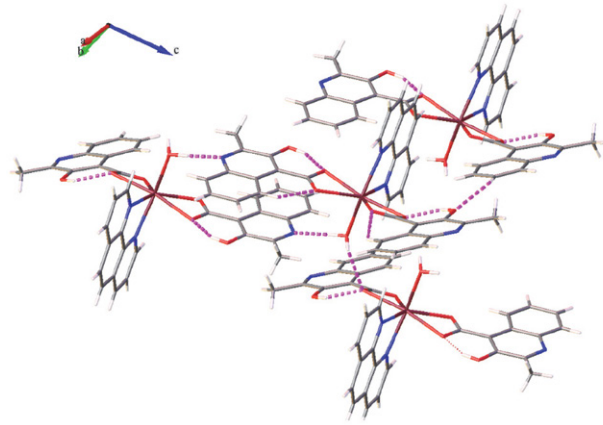

Figure 2. Hydrogen bonds in complex 1

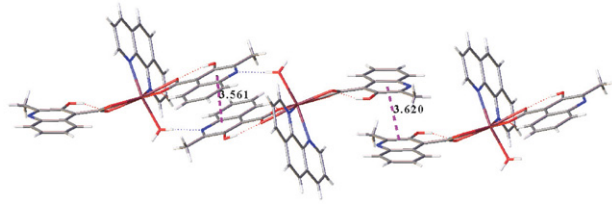

Figure 3. The π···π stacking interactions diagram of the complex 1

In the structure, there are two strong offset face-to-face π···π stacking interaction between *Cg*1···*Cg*1^{i} and *Cg*2···*Cg*2^{ii} (*Cg*1 is the ring C2–C4/C6/C11/N1; *Cg*2 is the ring C13–C15/C17/C22/N2) as shown in Figure 3. The centroid-centroid distance of *Cg*1···*Cg*1^{i} is 3.2620 Å, with a slippage distance of 0.941 Å, and with a dihedral angle of 0°. The centroid-centroid distance of *Cg*2···*Cg*2^{ii} is 3.567 Å, with a slippage distance is 1.098 Å, and with a dihedral Angle of 0° as shown in Table 4.

Table 4. π···π stacking interactions of the complex 1

Cg···*Cg*	Centroid-centroid distance (Å)	Slippage distance (Å)	Dihedral angle (Å)
*Cg*1···*Cg*1[i]	3.620	0.941	0.000
*Cg*2···*Cg*2[ii]	3.561	1.098	0.000

Symmetry codes: (i) 1 – *x*, 1 – *y*, 2 – *z*; (ii) 1 – *x*, 2 – *y*, 1 – *z*.

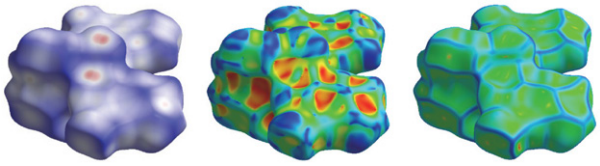

Figure 4. The Hirshfeld surface picture of the complex 1. From left to right are d_{norm}, shape index and curvature

3. 2. Hirshfeld Surface Analysis of the Complex 1

Hirshfeld surface analysis is gaining prominence as a technique in understanding the nature of intermolecular interactions within a crystal structure using a fingerprint plot. This allows easy identification of characteristic interactions throughout the structures or as a surface around the molecule. The size and shape of a Hirshfeld surface reflect the interplay between different atoms and intermolecular contacts in a crystal.[25,26] Crystal Explorer 3.1 program was used to calculate the force distribution of Hirshfeld surface molecules of the title complex, and the morphology, shape index and curvature diagram were obtained, as shown in Figure 4. The $d_{norm,}$ shape index and curve ranged from –0.6801 to 1.4037, –1.0000 to 1.0000, and –4.0000 to 0.4000, respectively. The d_{norm} surface is used

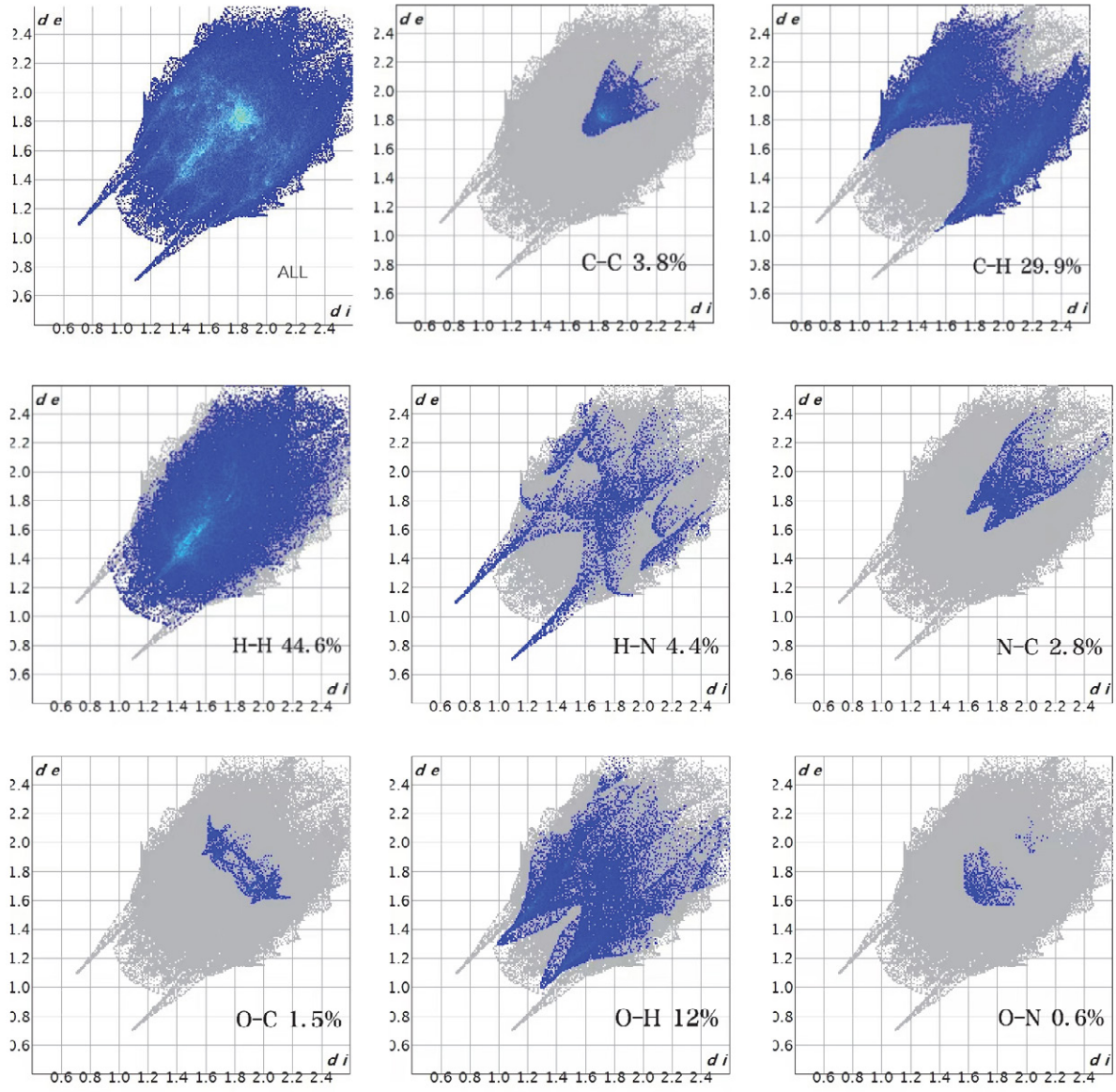

Figure 5. The 2D fingerprint of the complex 13.3 Photoluminescence measurements

for identification of very close intermolecular interactions. The red points on the d_{norm} surface of the title complex correspond to significant hydrogen bonding interaction. The shape index is most sensitive to very subtle changes in surface shape, the red triangle on the plane represents concave regions indicating atoms π···stacked molecule above them, and the blue represents convex regions indicating the ring atoms of the molecule inside the surface. The curvedness in the measurement of "how much shape".

The 2D fingerprint plots complement the Hirshfeld surfaces, quantitatively summarizing the nature and type of intermolecular contacts experienced by molecules in the crystal. The five main modes of action are H···H, C···H, O···H, H···N, C···C and H···N, as shown in Figure 5. Among them, the action of H···H is distributed in the middle region of the fingerprint, and its contribution to the surface of Hirshfield is the largest, reaching 44.6%, which is the most important mode of action. Followed by C···H, O···H, H···N, C···C and H···N, with a contribution ratio of 29.9%, 12%, 4.4% and 3.8%, respectively. C···H and O···H are conventional intramolecular hydrogen bonds, which are distributed in two-dimensional fingerprint region in a double wing shape. The distribution of the upper and lower spikes in the figure 5 corresponds to the donor of hydrogen bond and the acceptor of hydrogen bond (H···N and N···H).

The photoluminescence of complexes is increasingly gaining attention from scientists, making the study of photoluminescent materials from organic-inorgainc complexes of great significance.[27] Based on this, we performed fluorescence spectroscopic analysis of the title complex at room temperature, and the experimental results are shown in Figure 6.

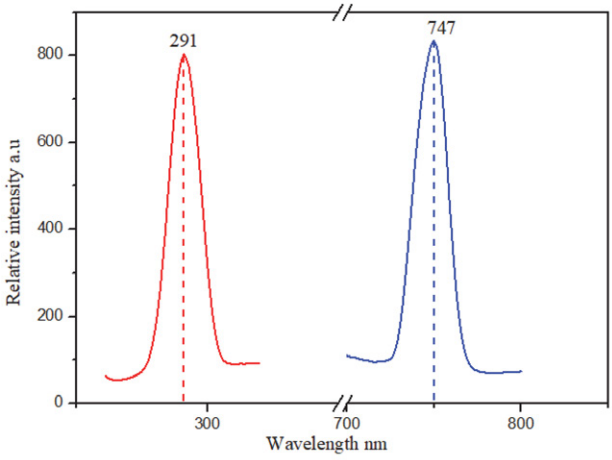

Figure 6. The solid-state excitation and emission spectra of the complex 1. The red is the emission spectrum, and the blue is the excitation spectrum

The complex **1** exhibits effective energy absorption in the wavelength range of 200–400 nm. When the excitation wavelength is 747 nm, there is obvious absorption at 291 nm. At 291 nm, the excitation spectrum has a corresponding absorption peak at 747 nm.

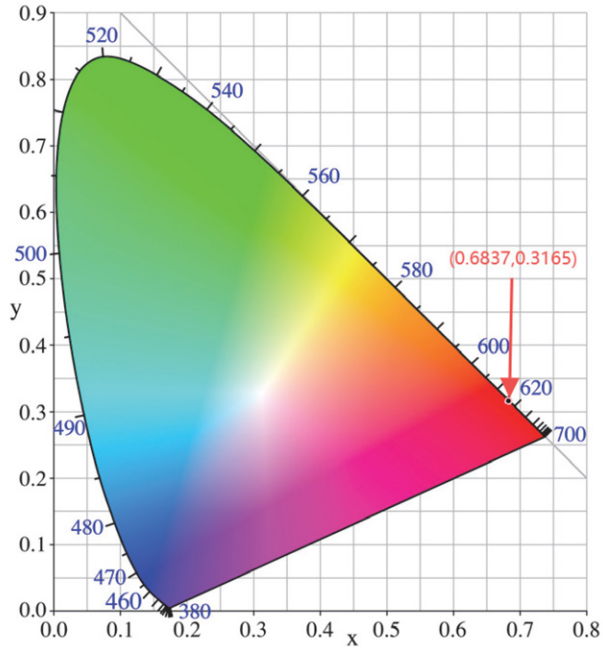

Figure 7. CIE chromaticity diagrams and chromaticity coordinates of the emission spectra of the complex 1

Solid state photoluminescence specter shows that they present a red emission band at 747 nm. The chromaticity coordinates of the title complex under radiation are calculated. The CIE estimate is $x = 0.6837$, $y = 0.3165$ (Figure 7). Therefore, we consider the complex **1** to be a promising red LED material.

3. 4. UV-vis Diffuse Reflection Spectra of Solid State

To study the optical properties of the crystal, the optical absorption properties of the crystal were measured by UV-vis diffuse reflection spectroscopy. At room temperature, using barium sulfate as 100% reflectance as a reference, the light absorption ability of the target complex was tested, and the band gap value of the material could be calculated by conversion. Energy band gap is an important concept to describe the distribution of electron energy states in solid materials, especially in crystalline materials.[28]

In terms of data processing, the following formula is used for derivation[29,30]

$$\alpha h\nu = B(h\nu - E_g)^m \quad (1)$$

where α is the molar absorption coefficient, h is Planck's constant, ν is the incident photon frequency, B is the proportionality constant, and E_g is the optical band gap of the semiconductor material.

According to Lambert-Beer law

$$A = \alpha bc \tag{2}$$

where A is the absorbance of the sample, b is the thickness of the sample, c is the concentration, where bc is a constant, if $B1 = (B/bc)^{1/m}$, formula (1) can be,

$$(Ahv)^{1/m} = B(hv - E_g) \tag{3}$$

$$E = hv = hc/\lambda \tag{4}$$

$$(Ahc/\lambda)^{1/m} = B(hc/\lambda - Eg) \tag{5}$$

there are different m values for different materials, and the relevant values can usually be obtained by referring to relevant literature (experience: n is ½ for direct bandgap semiconductors, n is 2 for indirect bandgap semiconductors).

Then the final formula is

$$(Ahc/\lambda)^2 = B(hc/\lambda - E_g) \tag{6}$$

where c is the speed of light, h is the Planck constant, and the photon energy unit is eV.

First, the wavelength λ-absorbance A data of the complex were obtained through solid state UV-VIS diffuse reflection spectroscopy experiment, as shown in the left side of Figure 8, then the corresponding Hv and $(Ahv)^2$ were calculated, and the corresponding Hv and $(Ahv)^2$ were plotted as shown in the right side of Figure 8. Finally, according to formula (6), when $(Ahc/\lambda)^2$ is equal to 0, the corresponding hc/λ is equal to E_g, that is, in the right side of Figure 8, the extreme point (x, y) is used as the tangent point as the tangent line, extrapolated to the horizontal axis ($y = 0$), and the intersection point is the band gap width value E_g.

The test results showed that the title complex showed light absorption in both ultraviolet and visible regions, and the prepared samples mainly showed absorption bands near 200 nm and 400 nm, corresponding to the absorption of transition metals in the MOF framework and ligand-based absorption. The energy band gap of the complex E_g = 2.32 eV is between metal and insulator, indicating that the complex **1** has semiconductor potential.

3. 5. Theoretical Calculation

In order to reveal the intrinsic fluorescence properties of Cd(II) complexes, we calculated them using the Gaussian09 program using TDDFT based on the B3LYP function (Cd as the basis set SDD and C, H, O and N as the basis set 6-31G*). The single-crystal X-ray diffraction data set of the complex **1** was used to truncate the ground-state

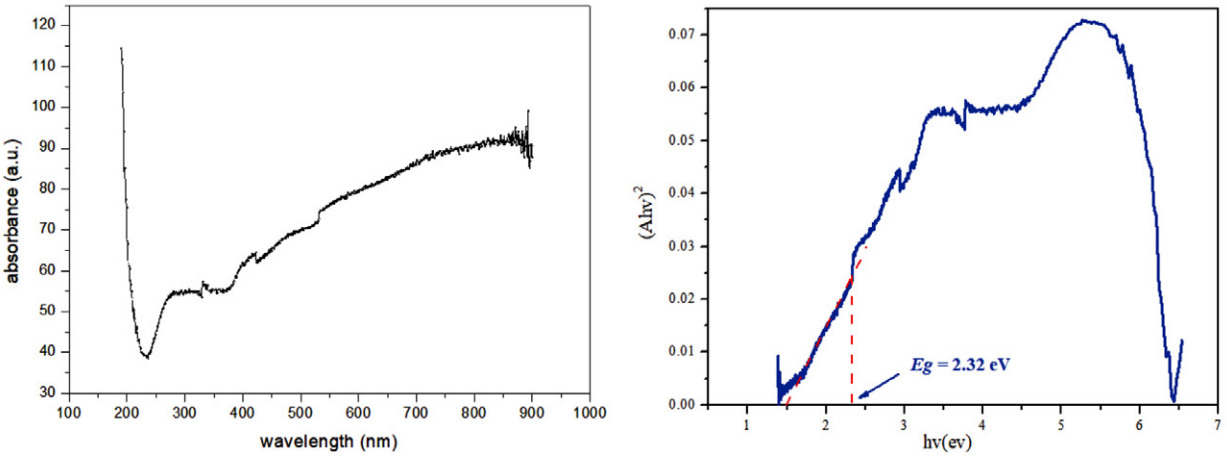

Figure 8. The UV-Vis spectra and the solid-state UV-Vis diffuse reflectance spectrum of the complex 1

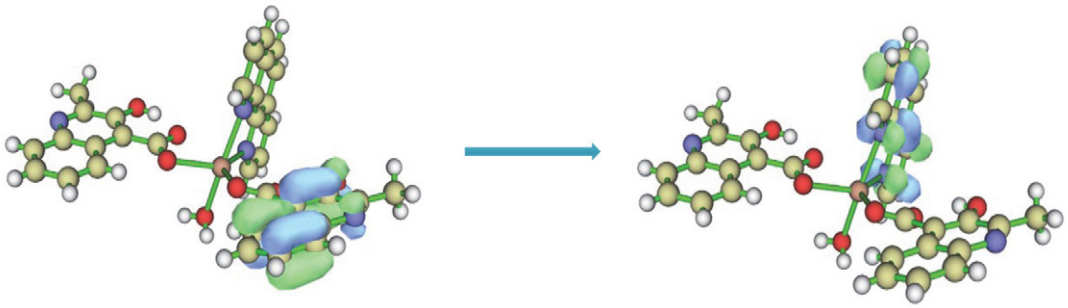

Figure 9. HOMO (left) and LUMO (right) of the complex 1

geometry for the calculations, the X-ray diffraction data for the title complex was not optimized further.[31–33] The characteristics of the highest occupied molecular orbital (HOMO) and the lowest unoccupied molecular orbital (LUMO) are shown in Figure 9.

The results show that the HOMO electron density distribution is located on the MCA^- ligand orbital, corresponding to the energy of –0.214699 a.u. (–5.842250 eV) in the π orbital, while the LUMO electron density distribution is completely located on the Phen ligand orbital. The corresponding energies are –0.098587 a.u. (–2.682690 eV). The HOMO–LUMO energy difference is 0.116112 a.u., that is 3.159559 eV and 304.851190 kJ/mol.

Based on this observation, the photoluminescent properties of the complex **1** can be attributed to the charge transfer between ligand and ligand (LLCT; from the HOMO of the π orbital of the MCA^- ligand to the LUMO of the π orbital of the Phen ligand. The calculated results agree well with the experimental results.

Supplementary Materials & Data Availability

Crystallographic data have been deposited with the Cambridge Crystallographic Data Center, CCDC 2384768. Copies of the data can be obtained free of charge from the Director, CCDC, 12 Union Road, Cambridge, CBZ, 1 EZ, UK; email: deposit@ccdc.cam.ac.uk or http://www.ccdc.cam.ac.uk.

Acknowledgements

The authors thank the National Natural Science Foundation of China (22168018), the National Natural Science Foundation of Jiangxi, China (20232BAB203048) and the National Natural Science Foundation of Jiangxi Ji'an, China for supporting this work.

Declaration of Competing Interest

The authors declare that they have no known competing financial interests or personal relationships that could have appeared to influence the work reported in this paper.

Data availability

Data will be made available on request.

4. References

1. B. D. S. Deeraj, J. S. Jayan, A. Raman, A. Asok, R. Paul, A. Saritha, K. Joseph, *Surf. Interfaces*. **2023**, *43*, 103574. **DOI:**10.1016/j.surfin.2023.103574
2. B. Jiang, C. W. Zhang, X. L. Shi, H. B. Yang, *Chinese. J. Polym. Sci*. **2019**, *37*, 372–382. **DOI:**10.1007/s10118-019-2216-1
3. A. Otero, J. Fernández-Baeza, A. Lara-Sánchez, L. F. Sánchez-Barba, *Coord. Chem. Rev.* **2013**, *257*, 1806–1868. **DOI:**10.1016/j.ccr.2013.01.027
4. C. Li, D. Wu, D. S. Zhang, L. L. Wang, X. P. Zhang, J. Liu, S. M. Zhang, T. L. Li, Z. F. Shi, Q. Lin, *Chinese J. Inorg. Chem*. **2019**, *35*, 376–384. **DOI:**10.11862/CJIC.2019.035
5. X. Cao, N. Feng, Q. Huang, Y. Liu, *ACS Appl. Bio Mater*. **2024.** **DOI:**10.1021/acsabm.3c01300
6. S. Banerjee, C. T. Lollar, Z. Xiao, Y. Fang, H. C. Zhou, *Trends Chem*. **2020**, *2*, 467–479. **DOI:**10.1016/j.trechm.2020.01.007
7. H. Chen, G. Lyu, Y. Yue, T. Wang, D. P. Li, H. Shi, J. Xing, J. Shao, R. Zhang, J. Liu, *J. Mater. Chem. C* **2019**, *7*, 7249–7258. **DOI:**10.1039/C9TC01520E
8. G. Y. Lv, T. W. Wang, W. Y. Wang, R. Zhang, J. Liu, *Chinese J. Inorg. Chem.* **2020**, *36*, 1669–1674. **DOI:**10.11862/CJC.2020.189
9. J. Zhang, W. Zhou, L. Yang, M. Dou, W. Qu, S. Lu, X. Chen, *Dyes Pigm*, **2024**, *229*, 112282. **DOI:**10.1016/j.dyepig.2024.112282
10. M. Tabatabaee, S. Tabatabaee, M. Dusek, M. Krupickova Pojarova, *Acta Crystallogr. A* **2011**, *67*, C617–C617. **DOI:**10.1107/S0108767311084418
11. L. J. Xu, C. M. Wang, K. Yu, C. X. Wang, B. B. Zhou, *Coord. Chem. Rev.* **2023**, *481*, 215044. **DOI:**10.1016/j.ccr.2023.215044
12. J. D. Rolfes, M. van Gastel, F. Neese, *Inorg. Chem.* **2020**, 59, 1556–1565. **DOI:**10.1021/acs.inorgchem.9b03474
13. J. C. Ott, D. Bürgy, H. Guan, L. H. Gade, *Acc. Chem. Res.* **2022**, 55, 857–868. **DOI:**10.1021/acs.accounts.1c00737
14. C. A. T. Zepeda, A. Coelho, O. Versiane, M. A. Mondragón, R. S. Pessoa, C. A. T. Soto, *J. Mol. Struct.* **2023**, *1287*,135618. **DOI:**10.1016/j.molstruc.2023.135618
15. P. Mantos, C. Ferrone, T. Ohta, P. Choudhury, S. Chowdhury, *Appl. Surf. Sci.* **2023**, 614, 156204. **DOI:**10.1016/j.apsusc.2022.156204
16. L. Ciołek, M. Chraniuk, P. Bollin, M. Biernat, M. Panasiuk, D. Nidzworski, B. Gromadzka, Z. Jaegermann, E. Pamuła, *Acta Bioeng. Biomech.* **2023**, *25*, 69–80. **DOI:**10.37190/ABB-02339-2023-02
17. É. Quarez, A. Jouhara, S. Grolleau, F. Dolhem, N. Dupré, P. Poizot, *CrystEngComm*. **2020**, *22*, 1653–1663. **DOI:**10.1039/C9CE01674K
18. X. G. Yi, X. N. Fang, J. Guo, J. Li, Z. P. Xie, *Acta Chim. Slov*. **2020**, *67*,507–515. **DOI:**10.17344/acsi.2019.5532
19. OD Rigaku (2022). *CrysAlis PRO.* Rigaku Oxford Diffraction, Yarnton, Oxfordshire, England.
20. G. M. Sheldrick, *Acta Crystallogr. A* **2008**, *64*, 112–122. **DOI:**10.1107/S0108767307043930
21. G. M. Sheldrick, *Acta Crystallogr. C* **2015**, *C71*, 3–8. **DOI:**10.1107/S2053229614024218
22. O. V. Dolomanov, L. J. Bourhis, R. J. Gildea, J. A. K. Howard, H. Puschmann, *J. Appl. Crystallogr.* **2009**, *42*, 339–341. **DOI:**10.1107/S0021889808042726
23. N. Palanisami, P. Rajakannu, R. Murugavel, *Inorg. Chim. Acta* **2013**, *405*, 522–531. **DOI:**10.1016/j.ica.2013.04.021
24. X. J. Zhang, Y. P. Tian, S. L. Li, M. h. Jiang, A. Usman, S.

Chantrapromma, H. K. Fun, *Polyhedron* **2003**, *22*, 397–402. **DOI:**10.1016/S0277-5387(02)01360-8
25. K. Z. Yang, R. Zou, X. G. Yi, J. B. Zhang, *Acta Chim. Slov*. **2023**, *70*, 310-317. **DOI:**10.17344/acsi.2023.8005
26. N. Abad, Y. Ramli, T. Hökelek, N. K. Sebbar, J. T. Mague, E. M. Essassi, *Acta Crystallogr. E* **2018**, *74*, 1648–1652. **DOI:**10.1107/S2056989018014561
27. M. H. You, M. H. Li, Y. M. Di, Y. W. Wang, M. J. Lin, *Dyes Pigm*. **2020**, *173*, 107943. **DOI:**10.1016/j.dyepig.2019.107943
28. F. D. E. Ghorabe, A. S. Novikov, P. V. Nesterov, A. R. Galina, A. E. Dudaev, E. I. Shishatskaya, E. V. Skorb, *Mater. Today Commun*. **2024**, *39*, 108886. **DOI:**10.1016/j.mtcomm.2024.108886
29. J. Tuac, R. Grigorovici, A. Vancu, *Phys. Stat. Sol.* **1966**, *15*, 627. **DOI:**10.1002/pssb.19660150224
30. E. A. Davis, N. F. Mott, *Philos. Mag*. **1970**, *22*, 903–822. **DOI:**10.1080/14786437008221061
31. H. U. Kim, S. Sohn, W. Choi, M. Kim, S. U. Ryu, T. Park, S. Jung, K. S. Bejoymohandas, *J. Mater. Chem. C* **2018**, *6*, 10640–10658. **DOI:**10.1039/C8TC04321C
32. W. Q. Zeng, W. Huang, C. H. He, R. Zou, W. K. Jin, X. G. Yi, K. Z. Yang, *J. Chem. Res*. **2023**, *47*, 1–9. **DOI:**10.1177/17475198231177955
33. N. H. Kwon, J. Park, X. Y. Jin, S. J. Kim, H. Kim, S. J. Hwang, *ACS Nano.* **2023**, 17, 23732–23745. **DOI:**10.1021/acsnano.3c07566

Povzetek

S solvotermalno metodo smo sintetizirali nov organsko-anorganski hibridni kadmijev kompleks [Cd(MCA)$_2$(Phen)(H_2O)] (MCA = anion 3-hidroksikinolin-4-karboksilne kisline; Phen = 1,10-fenantrolin) ter ga okarakterizirali z monokristalno rentgensko difrakcijo. Kompleks tvori dvodimenzionalno strukturo zaradi vodikovih vezi in π···π interakcij. Fotoluminiscenčni spekter v trdnem stanju kaže, da kompleks emitira v rdečem delu svetlobnega spektra, kar je mogoče pripisati prenosu naboja ligand-ligandi, kot kažejo časovno odvisni izračuni teorije gostotnostnega funkcionala. Spekter difuznega odboja kaže, da je energijska pasovna vrzel kompleksa 2,32 eV.